Signatures of progenitors of Type Ia supernovae

P. Hoeflich[1], S. Chakraborty[1], W. Comaskey[1], A. Fisher[1], B. Hristcov[1], D. Collins[1], T. R. Diamond[2], P. Dragulin[1], E. Y.Hsiao[1], and B. Sadler[3]

[1] Department of Physics, Florida State University, Tallahassee, FL 32306, USA
   e-mail: phoeflich@fsu.edu
[2] NASA Goddard Space Flight Center, Greenbelt, MD 20771, USA
[3] Western Governor's University, Dept. of Physics, Salt Lake City, UT 84107, USA

Abstract. Thermonuclear Supernovae (SNe Ia) are one of the building blocks of modern cosmology and laboratories for the explosion physics of White Dwarf star/s (WD) in close binary systems. The second star may be a WD (double degenerate systems, DD), or a non-degenerated star (SD) with a main sequence star, red giant or a helium star as companion (Branch et al. 1995; Nomoto et al. 2003; Wang & Han 2012). Light curves and spectra of the explosion look similar because a 'stellar amnesia' (Höflich et al. 2006). Basic nuclear physics determines the progenitor structure and the explosion physics, breaking the link between progenitor evolution, and the explosion, resulting in three main classes of explosion scenarios: a) dynamical merging of two WD and a heating on time scales of seconds (Webbink 1984; Isern et al. 2011), b) surface helium detonations on top of a WD which ignite the central C/O by a detonation wave traveling inwards (Nomoto 1982; Hoeflich & Khokhlov 1996; Kromer et al. 2010); c) compressional heating in an accreting WD approaching the Chandrasekar mass on time of up to 10^8 years which may originated from SD and DD systems (Whelan & Iben 1973; Piersanti et al. 2003). Simulations of the explosions depend on the inital conditions at the onset of the explosions, namely the mass and angular momentum of the WD(s). For all scenarios, diversity in SNe Ia must be expected because the WD originates from a range of Main Sequence masses ($M_{MS} < 8M_\odot$) and metallicities Z. Moreover, there is growing evidence that magnetic fields B may have to be added to the 'mix'. Only with recent advances in observations ranging from X-ray to radio, high precision spectroscopy, polarimetry and photometry and in the time-domain astronomy we obtain constraints for progenitor, on the explosion scenarios and links emerge between the progenitors and their environment with LCs and spectral signatures needed for high precision cosmology. It is too early to give final answers but we present our personal view. We will give some examples from the theory point of view and discuss future prospects with upcoming ground based, ELT, GMT and space based such as JWST, Euclide and WFIRST instruments.

Key words. Supernovae: Progenitors, Spectra, Light Curves – Cosmology

1. Introduction

The majority of Type Ia supernovae appears to be rather homogeneous with a well defined brigthness decline ratio relation Δm_{15} (Phillips 1993) and similar spectra.

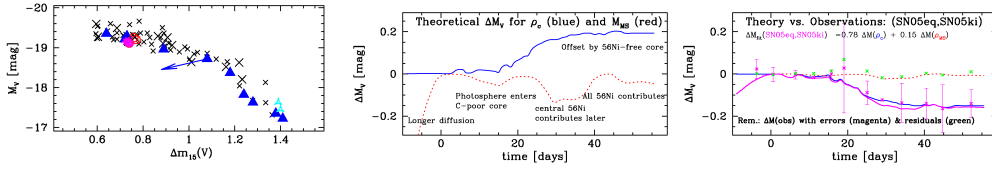However, thermonuclear explosions are a very diverse group objects as exempli-

Fig. 1. Δm_{15} relation (*left*) and differential analysis of SNe Ia pairs (*middle* and *right*). DDT models reproduce both collective and individual properties of SN Ia observations. *Left:* Δm_{15} of 45 SNe Ia from the CSP-I sample are compared to theoretical values for delayed detonation models (blue triangles) and models with different central densities ρ_c of the WD (magenta) (Hoeflich 2006). The arrow shows the shift when mixing all layers up to 12 500 km s^{-1} and would destroy a tight relation. *Middle, Right*: Template differential LCs ΔM_V for $M_{MS} = 5 vs 7 M_\odot$ and a central WD density $\rho_c = 2 vs .6 \times 10^9$ g cm^{-3}. An example of template fitting of the SNe 2005eq and 2005ki is shown on the right using both the ρ_c and M_{MS} components (Sadler et al. 2012). These two SNe differ mostly in their central densities and show little difference in their main-sequence masses. Note that the residuals are less than 0.01 mag (green crosses).
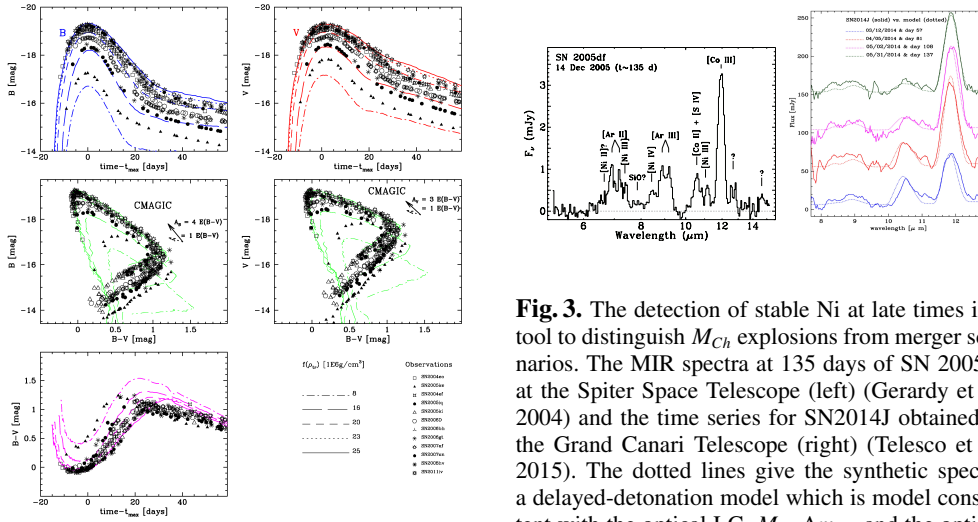

Fig. 2. Comparison between well-observed SNe Ia of CSP-I and our theoretical DD models. Varying the amount of deflagration burning describes the observed light, color and color-magnitude curve

Fig. 3. The detection of stable Ni at late times is a tool to distinguish M_{Ch} explosions from merger scenarios. The MIR spectra at 135 days of SN 2005df at the Spiter Space Telescope (left) (Gerardy et al. 2004) and the time series for SN2014J obtained at the Grand Canari Telescope (right) (Telesco et al. 2015). The dotted lines give the synthetic spectra a delayed-detonation model which is model consistent with the optical LC, M_V, Δm_{15}, and the optical spectra for SN2014J.

fied by two recently identified new subclasses, SNe Iax (Li et al. 2011) and super-Chandrasekhar SNe Ia (Howell et al. 2006). Further evidence comes from the large number of 'odd-balls': For example SN1991t-like SNe show low Δm_{15} (Mueller et al. 1991), and comparably weak layers of intermediate mass elements (Krisciunas et al. 2004). SN2000cn-like SNe show very high ionization in spectra but large Δm_{15}, SN2001ay-like SNe show lower Δm_{15} than any SNe Ia known combined with a fast rise and normal brightness (Krisciunas et al. 2011; Baron et al. 2012). All LC data are based on the first Carnegie Supernovae Program release CSP-I (Contreras et al. 2010). **Evidence that M_{Ch} mass explosions may provide the dominant component** though, likely, all explosion scenarios contribute to the SNe Ia.
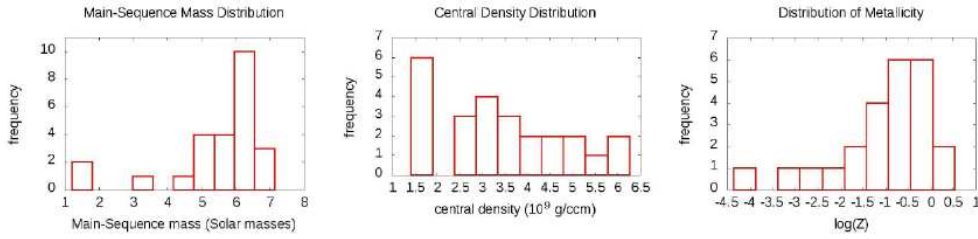
Fig. 4. Distribution of main sequence masses of the progenitors, the central density of the WD at the time of the explosion, and the metallicity based on component analyses. Note that the current data allow to identify trends but the error bars are quiet large for individual SNe Ia (Sadler 2012).
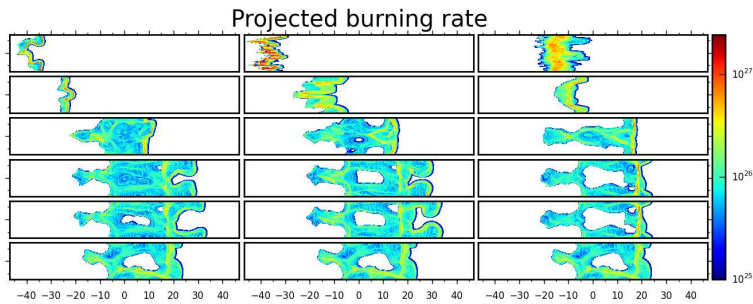

Fig. 5. Influence of B fields on the nuclear burning front is shown at $0.6 sec$ in a flux tube of 240 km for conditions typical for a WD with $C/O = 1$ and $\rho_c = 10^8$ g cm^{-3} at a comoving distance of about 1,000 km s^{-1} using Enzo. We show the normalized burned fraction for runs, with the burning front traveling to the right, which have differing B field strength and orientation but are otherwise identical (Hristov et al. 2016). The rows correspond to magnetic field strengths of $B = 10^{12}$, 10^{11}, 10^{10}, 10^9, 10^8, and 0 G. The direction of the initial B-field is parallel to the flux tube (*left*), at 45° to the flux tube (*middle*), and orthogonal to the flux tube (*right*). B emerge as important component with $B > 10^{4...6}G$ both from late-time NIR spectra and LCs (Hoeflich et al. 2004; Penney & Hoeflich 2014; Diamond et al. 2015), and may suppress excessive strong Rayleigh-Taylor mixing which would degrade a tight Δm_{15} relation (Fig. 1).

Within M_{Ch} explosions, those possessing a transition from a deflagration to a detonation front (DDT), called delayed-detonation models (Khokhlov 1991), have been found to reproduce the optical and infrared (IR) light curves and spectra of individual typical SNe Ia reasonably well including the time evolution and statistical properties (Hoeflich et al. 2013), and the solar abundance pattern of ^{48}Ca (Thielemann et al. 2002). A recent analysis of the 45 best SNe Ia of CSP-I shows that Δm_{15} (Fig. 1) and color-magnitude diagrams (Fig. 2) smoothly sample the distribution without 'brakes', and the M_{Ch} mass models can re-

produce the resulting relations (Hoeflich et al. 2017, submitted).

2. The SNe Ia-Progenitor Connection

Linking SNe Ia to their Progenitors: The WD progenitor introduces a diversity for all explosion scenarios. Variables are the a) primordial metallicity, Z; b) C/O ratio as a function of mass coordinate in the WD, which mostly depends on the main sequence mass M_{MS} because mostly determines the size of the central He-burning core during the stellar evolution (Domínguez et al. 2001); c) central
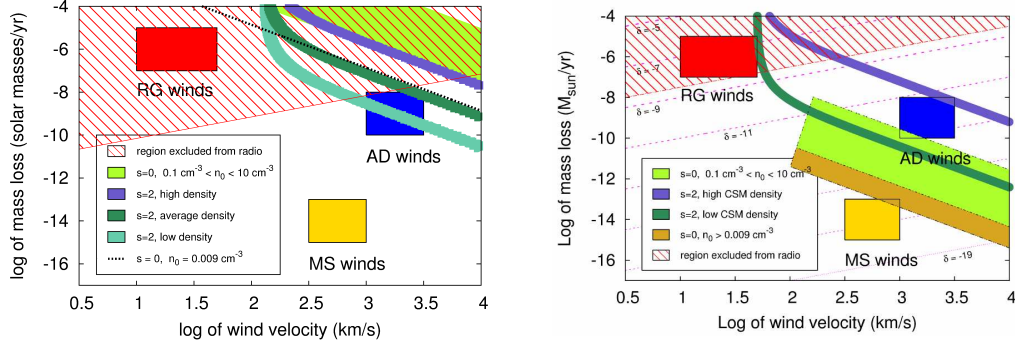
Fig. 6. Parameters for the enviroment of SN 2014J and SN 2006X produced by a mass-loss characterized by a mass loss rate $\dot{m}$ and wind-speed v_w and wind parameters typical for red-giant (RD), main-sequence star (MS) and accretion disks (AD) winds. The red area is the forbidden area based on radio and X-ray observations. Lines of constant radio luminosity are given by $\delta = log_{10}(\dot{m}/v_w)$. The green area indicates the allowed range for constant density environments with particles densities between 0.1 and 10 cm^{-3}. The thick lines correspond to environments produced with an r^{-2} power law as may be produced by winds during stellar evolution. X-ray, radio and narrow spectral lines favor cavities formed due to winds from an accretion disk, and rule out RSG as donor stars (Dragulin & Hoeflich 2016).

Object	Host	M_B	$dm_{15,B}$	M_V	$dm_{15,V}$	$E_{B-V,Gal,Host}$	$E_{B_V}^{CM}, R_B, \Delta R_V$	$(B-V)_o(a,b)$	$m-M$	$m-M_{ave,min,max}$
SN2005M	NGC2930	-19.22	0.84	-19.18	0.58	0.032 ,0.06	0.046, 2.5, 0.7	-0.022, -0.030	35.23	35.21,24.82,35.06
SN2004eo	NGC6928	-18.70	1.52	-18.82	0.82	0.11 ,-	0.128, 1.8, 1.3	0.033, -0.018	34.36	33.74,32.80,34.66
SN2005am	NGC2811	-18.94	1.52	-18.91	0.85	0.043 ,0.053	0.152, 1.5, 0.5	-0.103, -0.030	32.348	32.63,31.66,35.26
SN2005ke	NGC1371	-17.62	1.76	-18.16	1.27	0.023 ,0.263	0.223, 3.3, 0.5	0.430, 0.460	31.317	32.09,31.91,32.49
SN2004ef	UGC12158	-18.83	0.81	-18.90	1.38	0.054 ,0.158	0.154, 2.9, 0.7	0.026, -0.018	35.71	35.40,34.78,35.53
SN2005el	NGC1819	-19.24	0.85	-19.22	1.35	0.11 ,0.015	0.110, 3.6, 0.5	-0.062, -0.030	34.33	33.97,33.29,34.29
SN2005iq	MGC0108	-19.26	1.25	-19.14	0.80	0.022 ,0.040	0.022, 1.5, 0.5	-0.011, -0.012	36.00	35.92,35.26,36.20
SN2005ki	NGC3332	-19.01	1.37	-19.00	0.82	0.032 ,0.016	0.032, 1.9, 0.5	0.003, 0.010	34.70	34.47,31.73,34.91
SN2006D	MGC0133	-18.73	1.39	-18.86	0.87	0.046 ,0.134	0.050, 3.8, 1.5	0.127, 0.046	32.90	32.73,32.23,33.01
SN2006X	NGC4321	-18.34	1.12	-18.90	0.64	0.026 ,1.360	1.190, 1.7, 1.0	0.069, -0.030	32.20	31.04,30.20,32.23
SN2006bh	NGC7329	-18.96	1.43	-18.92	0.81	0.026 ,0.037	0.040, 1.5, 0.5	-0.026, -0.030	33.68	33.20,31.60,33.68
SN2006gt	+	-18.51	1.64	-18.65	1.10	0.032 ,0.074	0.059, 3.1, 1.2	0.137 0.084	36.72	-
SN2007S	UGC5378	-19.00	0.95	-19.17	0.59	0.028 ,0.478	0.386, 3.0, 0.9	-0.040 -0.030	34.12	33.92,33.36,34.22
SN2007af	NGC5584	-18.71	1.20	-18.75	0.67	0.039 ,0.178	0.099, 3.9, 1.0	-0.032 -0.030	32.18	31.78,30.69,32.67
SN2007ai	MGC....	-17.99	-	-18.26	-	0.033 ,0.160	0.113, 3.2, 0.6	0.126 -0.030	36.52	35.69,35.09,36.01
SN2007le	NGC7721	-18.5, 0.9	0.97	-18.67	0.69	0.033 ,0.388	0.300, 1.8, 0.9	0.000 -0.030	32.64	31.68,31.19,32.24
SN2007on	NGC1404	-18.43	1.86	-18.57	1.09	0.012 ,¡0.007	0.012, 3.1, 0.5	0.150 0.124	31.38	31.40,30.67,32.23
SN2008bc	KK1524	-18.77	0.82	-18.88	0.67	0.026 ,¡0.019	0.154, 3.9, 0.7	0.046 -0.030	34.43	34.04
SN2008fp	++	-18.56	0.84	-18.97	0.65	0.20 ,0.578	0.590, 2.3, 1.0	0.108 -0.030	32.58	31.82
SN2008hv	NGC2765	-19.12	1.33	-19.19	-	0.032 ,0.074	0.032, 3.9, 0.5	0.063 -0.030	34.03	33.82,33.57,33.99
SN2011iv*	NGC1404	-18.67	1.72	-18.68	0.97	0.012 , -	0.012, 1.9, 0.5	0.068 0.047	31.25	31.40,30.67,32.23

Fig. 7. Properties for our CSP-I SNe Ia and their host galaxies. M_V, M_B, Δm_{15} and E_{B-V} of the Galaxy and Host has been taken directly from SNooPy-fits (Burns et al. 2015). E_{B-V} for the galactic and host galaxy is given as indicator for low and high reddening, respectively, which show a wide range for R_V between 1 to 3.8 (Burns et al. 2011). In addition, we give our models fits for $m-M$, E_{B-V}, R_B, and ΔR_{B-V} using CMAGIC and theoretical templates. The $(B-V)_o(V_{max})$ implied by CMAGIC (a) and actual values of the models (b) which may serve as error estimate.

density ρ_c of the WD at the time of the explosion is directly correlated to $M(WD)$ for quasi-hydrostatic configurations, the starting point of M_{Ch} and Helium-triggered explosions.

Using theoretical templates, component analyses of the difference in bright Δm of pairs of observed SNe Ia allows to derive those parameters (Fig.4). Higher M_{MS} means less

energy release during the explosion, and a smaller expansion rate. Δm rises slower due to the smaller geometrical dilution. Eventually, Δm becomes close to zero when all instant energy deposition contributes to the LC. Variations in ρ_c mostly affect the size of the core region with little or no ^{56}Ni for $M_{WD} > 1.2 M_\odot$ because electron capture results in a shift of the Nuclear Statistical Equilibrium from ^{56}Ni toward neutron rich isotopes, e.g. ^{58}Ni and ^{57}Co (Brachwitz et al. 2000). Because expansion and diffusion time scales are both about equal at maximum light for models with the same stretch s, Δm remains small but, at later times, lack of ^{56}Ni causes an off-set in Δm. As independent measure for ρ_c, unblended NIR lines profiles become broader with ρ_c and require large B-fields (Hoeflich et al. 2004; Diamond et al. 2015) (Fig.5), and late-time MIR spectra show stable ^{58}Ni (Fig.3).

Note that the brightness in the U-band is sensitive to Z (Hoeflich et al. 1998; Lentz et al. 2001; Sauer et al. 2008). Statistical analysis of LCs suggests a broad peak around $1/3 Z_\odot$ for the CSP sample (Sadler 2012; Sadler et al. 2012). However, we cannot expect simple relations between Z and $(U - V)$ because U and the UV are equally sensitive to other quantities, such as mixing and interactions with the environment (Gerardy et al. 2004).

Signatures of the Progenitor Systems: The stellar environment will shed light on the evolutionary history of the progenitor and progenitor systems. It can be expected to consist of three main components: 1) Some matter bound in the progenitor system at the time of the explosion. It may originating from the accretion disk and be shed from the donor star 2) the wind from the WD, accretion disk and donor star for SD and wind from the Roche-lobe prior to the phase of dynamical merging; for DDs, and 3) the interstellar medium (ISM).

There is clear evidence for interaction with the matter within the progenitor system. Within the explosion of M_{Ch} mass WDs, hydrodynamic calculations have shown that the expanding supernova material wraps around the companion star and may pull off several tenths of a solar mass of material (Marietta et al. 2000; Kasen et al. 2009). Another source of

matter is the accretion disk material (Gerardy et al. 2003; Quimby et al. 2007).

At intermediate distances of up to several light years and in case of M_{Ch} mass explosions, the environment may be dominated by the wind from the donor star, the accretion disk or, for high accretion rates, by the wind from the WD, or the interstellar material (ISM). A number of possible signatures of the interaction which, however, is mostly illusive with limits down to $< 10^{-3} particle/cm^3$ (Chugai 1986; Schlegel 1995) for direct detection. However, evidence of a link between SNe Ia and the environment comes from narrow, time-dependent, blue-shifted NaD absorption line (D'Odorico et al. 1989) and circumstellar dust shells at distances of up to several hundred parsecs (Hamuy et al. 2000; Crotts & Yourdon 2008; Rest et al. 2008). In the framework of self similar solutions for ejecta/ISM interactions (Chevalier 1982) and based on X-ray and radio-observations combined with narrow high resolution spectra, Dragulin & Hoeflich (2016) found that virtually all scenarios produce a low-density cocoon with a typical scale of 0.1 to 10 lyrs depending on the progenitor wind and, thus, providing constrains on the progenitor systems (Fig. 6). The following picture of the environment emerge: SNe Ia are surrounded by a cocoon with a much lower environment than the ISM often, separated by a higher density region which produces NaD and may contain dust. The color-diagram allows for independent fits of colors, distances and reddening laws. For highly reddened SNe Ia, our analysis suggest smaller $R_V \approx 2$ and possibly different reddening laws than commonly adopted for our Galaxy (Cardelli et al. 1989) (Table 7).

References

Baron, E., Hoeflich, P., Krisciunas, K., et al. 2012, ApJ, 753, 105

Brachwitz, F., Dean, D., Hix, W. R., et al. 2000, ApJ, 536, 934

Branch, D., et al. 1995, PASP, 107, 1019

Burns, C. R., Stritzinger, M., Phillips, M. M., et al. 2011, AJ, 141, 19

Burns, C. R., Stritzinger, M., Phillips, M. M., et al. 2014, ApJ, 789, 32

Burns, C. R., Stritzinger, M., Phillips, M. M., et al. 2015, SNooPy: TypeIa supernovae analysis tools, Astrophysics Source Code Library

Cardelli, J. A., Clayton, G. C., & Mathis, J. S. 1989, ApJ, 345, 245

Chevalier, R. A. 1982, ApJ, 258, 790

Chugai, N. N. 1986, Soviet Ast., 30, 563

Contreras, C., Hamuy, M., Phillips, M. M., et al. 2010, AJ, 139, 519

Crotts, A. P. S. & Yourdon, D. 2008, ApJ, 689, 1186

Diamond, T. R., Hoeflich, P., & Gerardy, C. L. 2015, ApJ, 806, 107

D'Odorico, S., di Serego Alighieri, S., Pettini, M., et al. 1989, A&A, 215, 21

Domínguez, I., Hoeflich, P., & Straniero, O. 2001, ApJ, 557, 279

Dragulin, P. & Hoeflich, P. 2016, ApJ, 818, 26

Gerardy, C. et al. 2003, ApJ, 607, 391

Gerardy, C. L., Hoeflich, P., Fesen, R. A., et al. 2004, ApJ, 607, 391

Hamuy, M., Trager, S. C., Pinto, P. A., et al. 2000, AJ, 120, 1479

Hoeflich, P. 2006, Nuclear Physics A, 777, 579

Hoeflich, P. & Khokhlov, A. 1996, ApJ, 457, 500

Hoeflich, P., Wheeler, J. C., & Thielemann, F.-K. 1998, ApJ, 495, 617

Hoeflich, P., Gerardy, C. L., Nomoto, K., et al. 2004, ApJ, 617, 1258

Höflich, P., Gerardy, C. L., Marion, H., & Quimby, R. 2006, New Astron. Rev., 50, 470

Hoeflich, P., Dragulin, P., Mitchell, J., et al. 2013, Frontiers of Physics, 8, 144

Howell, D. A., Sullivan, M., Nugent, P. E., et al. 2006, Nature, 443, 308

Hristov, B., et al. 2016, American Astronomical Society Meeting Abstracts, 227, 237.16

Isern, J., Hernanz, M., & José, J. 2011, in Astronomy with Radioactivities, ed. R. Diehl, D. H. Hartmann, & N. Prantzos eds. (Springer, Berlin), Lecture Notes in Physics, 812, 233

Kasen, D., Röpke, F. K., & Woosley, S. E. 2009, Nature, 460, 869

Khokhlov, A. M. 1991, A&A, 245, L25

Krisciunas, K., Suntzeff, N. B., Phillips, M. M., et al. 2004, AJ, 128, 3034

Krisciunas, K., Li, W., Matheson, T., et al. 2011, AJ, 142, 74

Kromer, M., Sim, S. A., Fink, M., et al. 2010, ApJ, 719, 1067

Lentz, E. J., Baron, E., Branch, D., & Hauschildt, P. H. 2001, ApJ, 557, 266

Li, W., Bloom, J. S., Podsiadlowski, P., et al. 2011, Nature, 480, 348

Marietta, E., Burrows, A., & Fryxell, B. 2000, ApJs, 128, 615

Mueller, E., Hoeflich, P., & Khokhlov, A. 1991, A&A, 249, L1

Nomoto, K. 1982, ApJ, 257, 780

Nomoto, K., Uenishi, T., Kobayashi, C., et al. 2003, in From Twilight to Highlight: The Physics of Supernovae, ed. W. Hillebrandt & B. Leibundgut (Springer, Berlin), 115

Penney, R. & Hoeflich, P. 2014, ApJ, 795, 84

Phillips, M. M. 1993, ApJ, Letters, 413, L105

Piersanti, L., et al. 2003, ApJ, 598, 1229

Quimby, R., Hoeflich, P., & Wheeler, J. C. 2007, ApJ, 666, 1083

Rest, A., Matheson, T., Blondin, S., et al. 2008, ApJ, 680, 1137

Sadler, B. 2012, Master's thesis, Florida State University

Sadler, K., Hoeflich, P., Baron, E., et al. 2013, in Binary Paths to Type Ia Supernovae Explosions, R. Di Stefano, M. Orio, M. Moe eds. (Cambridge Univ. Press, Cambridge), IAU Symp., 281, 309

Sauer, D. N., Mazzali, P. A., Blondin, S., et al. 2008, MNRAS, 391, 1605

Schlegel, E. M. 1995, Reports on Progress in Physics, 58, 1375

Telesco, C. M., Hoeflich, P., Li, D., et al. 2015, ApJ, 798, 93

Thielemann, F.-K., Argast, D., Brachwitz, F., et al. 2002, Ap&SS, 281, 25

Wang, B. & Han, Z. 2012, New Astron. Rev., 56, 122

Webbink, R. F. 1984, ApJ, 277, 355

Whelan, J. & Iben, I. J. 1973, ApJ, 186, 1007